PHYSICAL REVIEW B **85**, 161103(R) (2012)

Elastic shells with high-contrast material properties as acoustic metamaterial components

Theodore P. Martin,[1] Christopher N. Layman,[2] Kimberly M. Moore,[1] and Gregory J. Orris[1]
[1]*Acoustics Division, Naval Research Laboratory, Washington, DC 20375, USA*
[2]*National Research Council, Washington, DC 20001, USA*
(Received 17 January 2012; revised manuscript received 13 March 2012; published 19 April 2012)

We analyze the acoustic multiple-scattering properties of fluid-filled, elastic cylindrical shells with highly contrasting material properties, and we find for a water background that air-filled shells homogenize into high-bulk modulus, low-density effective fluids. With the exception of a few local resonances spanning very narrow band windows, we find that for common elastic materials the shells are indistinguishable from their effective fluid counterparts for wavelengths larger than the shell's outer diameter. Furthermore, we find that when the elastic shell is composed of a material with impedance larger than water, there will be a specific shell thickness for which the effective fluid properties become impedance-matched. Finally, we demonstrate that the shells can be used as constituent components in regular lattices to create homogenized acoustic metamaterial devices.

DOI: 10.1103/PhysRevB.85.161103 PACS number(s): 81.05.Xj, 43.20.+g, 43.40.+s

Research efforts in the field of subwavelength structured composites, termed metamaterials, have significantly expanded the scope of optical and acoustic devices. In the acoustic and elastodynamic domains, unconventional device applications such as hyperlensing,[1] scattering reduction,[2–4] and wave rectification[5,6] have been recently demonstrated. Proposals in transformational acoustics (TA) promise many additional design possibilities, including three-dimensional scattering reduction,[7–9] wave-rotation/conversion,[10,12] and perfect absorption.[13] However, these proposals also reflect the core experimental difficulties encountered in the field; the constituent property requirements are either highly anisotropic (i.e., in the form of pentamode materials[9]) and/or extreme in their magnitude[7,8,14] beyond what is currently available. The approximation schemes used for coordinate transformations[11,12,14,15] often require constituent materials with simultaneously high stiffness and low density, a property that is typically restricted to highly anisotropic materials such as woods[12] or composites.[2,16] In addition, TA and other metamaterial applications (e.g., lensing[12,17]) attain optimal performance when these extreme constituent properties are also transparent with respect to the wave propagation medium, further restricting the search for viable material solutions.

Here we focus on the development of thin-walled, fluid-filled elastic shells as metamaterial components. Scattering from thin elastic shells has been thoroughly investigated using a variety of techniques for more than a century,[18] but it has not been considered in the context of metamaterials until recently. Elastic shells have been commonly exploited for their local resonances,[19] which provide functionality to sonic crystal filters,[20–22] resonant transmission enhancement,[23] and negative-valued media.[24–26] However, local resonances are inherently narrow in bandwidth and can be accompanied by high radiative loss, limiting their use to certain applications. Using multiple-scattering theory[27,28] (MST), we investigate instead the broadband functionality of elastic shells away from these resonances at wavelengths larger than the shell diameter, thus allowing for an effective-medium description.[29,30]

We concentrate on elastic cylindrical shells with material properties that contrast highly with those of the fluid core in order to obtain the extreme constituent properties required by metamaterial applications. We demonstrate that for a water background, stiff elastic shells containing a low-density fluid (air) are analogous to an effective fluid with high bulk modulus (B) and low density (ρ). Furthermore, the resultant effective properties can be tuned using the shell thickness and can achieve transparency at a specific thickness. It has previously been shown[12,17,31] that functionally graded, anisotropic fluidlike properties can be approximated by a periodic arrangement of mixed elastic scatterers, which operate in the homogenization limit. An effective-medium description of the elastic shells makes them appropriate as components in these periodic lattices, greatly expanding the accessible range of material properties with the additional advantage of transparency.

Our numerical results are obtained using multiple-scattering theory for radially stratified cylindrical shells.[27,28] The total pressure $P(r,\theta,z)$ at normal incidence in the vicinity of a fluid-filled, elastic cylindrical shell of outer diameter d and thickness h can be written as[27,30]

$$P = \sum_{q=-\infty}^{\infty} A_q^0 \left[J_q(k_f r) + [\mathcal{R}^{\mathcal{S}}]_q H_q^{(1)}(k_f r) \right] e^{iq\theta}, \quad (1)$$

$$[\mathcal{R}^{\mathcal{S}}]_q = [\mathcal{R}_{fe}]_q + [\mathcal{T}_{ef}]_q [\mathcal{R}_{ec}]_q [\mathcal{S}]_q, \quad (2)$$

$$[\mathcal{S}]_q = ([I] - [\mathcal{R}_{ef}]_q [\mathcal{R}_{ec}]_q)^{-1} [\mathcal{T}_{fe}]_q, \quad (3)$$

where k_f and A_q^0 are the incident wave number and wave coefficients of order q in the background fluid, respectively. Bracketed terms designate identity $[I]$, transmission $[\mathcal{T}]$, and reflection $[\mathcal{R}]$ matrix elements governing waves incident on the shell's radially symmetric boundaries. Wave coefficients $[\mathcal{R}^{\mathcal{S}}]_q$ give the total reflection from the shell, while $[\mathcal{S}]_q$ are convergent sums over an infinite number of multiple reflections between the boundaries of the shell.[27] Equations (2) and (3) use a convention where the first index designates the region where the wave originates, and the second index designates the region of scattering interaction.[27] For the elastic shell there are three regions: the fluid background f, the elastic shell e, and the fluid core c. For example, $[\mathcal{R}_{ec}]_q$ describes the reflection of a wave within the elastic shell after interacting with the core's boundary. In the general case of elastic media, the MST elements $[\mathcal{R}^{\mathcal{S}}]_q$ are a set of 2×2 matrices describing coupling between the longitudinal (l) and transverse (t) modes.

A fluid background medium only supports l modes, and $[\mathcal{R}^{\mathcal{S}}]_q$ is therefore a scalar set. However, inside the elastic shell the t modes cannot be ignored and the reflection matrices such as $[\mathcal{R}_{ec}]_q$ take the form[28]

$$\begin{Bmatrix} B_q^{(l)} \\ B_q^{(t)} \end{Bmatrix} = \begin{bmatrix} \mathcal{R}_{ec}^{(ll)} & \mathcal{R}_{ec}^{(lt)} \\ \mathcal{R}_{ec}^{(tl)} & \mathcal{R}_{ec}^{(tt)} \end{bmatrix}_q \begin{Bmatrix} A_q^{(l)} \\ A_q^{(t)} \end{Bmatrix}, \tag{4}$$

where $A_q^{(l,t)}$ and $B_q^{(l,t)}$ represent incident and reflected scattering coefficients, respectively. Likewise, the transmission terms are 2×1 matrices that couple the elastic shell modes into the fluid.

To obtain the effective fluid properties of the elastic shells, the multiple-scattering result is compared to the two lowest-order transfer-matrix elements T_q of a uniform fluid cylinder with outer diameter d in the long-wave limit,[29,30]

$$\lim_{k\to 0} T_0 \approx T_0^{k\to 0} \equiv \frac{i\pi d^2}{16}\left[\frac{1}{\overline{B}_{\text{eff}}} - 1\right] k_f^2 \simeq \lim_{k\to 0}[\mathcal{R}^{\mathcal{S}}]_0, \tag{5}$$

$$\lim_{k\to 0} T_1 \approx T_1^{k\to 0} \equiv \frac{i\pi d^2}{16}\left[\frac{\overline{\rho}_{\text{eff}} - 1}{\overline{\rho}_{\text{eff}} + 1}\right] k_f^2 \simeq \lim_{k\to 0}[\mathcal{R}^{\mathcal{S}}]_1, \tag{6}$$

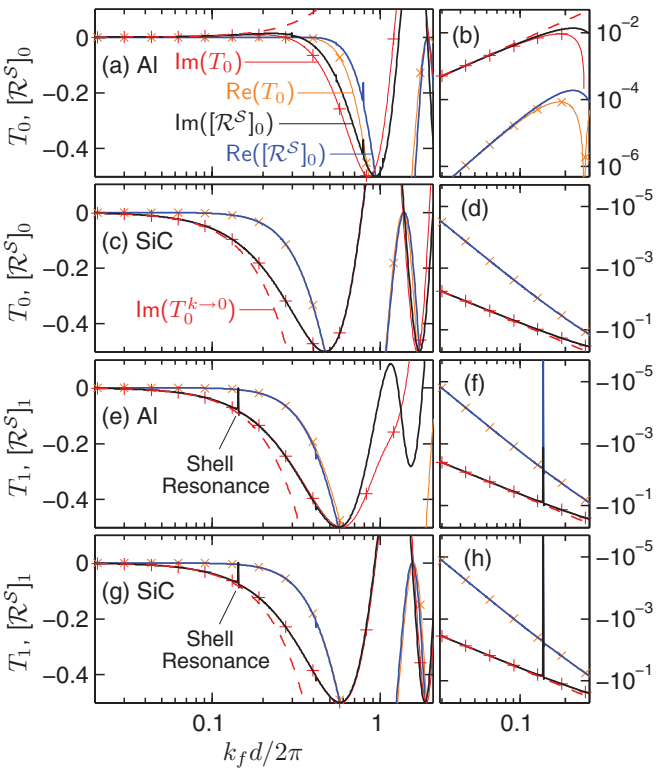

FIG. 1. (Color) Scattering matrix elements $[\mathcal{R}^{\mathcal{S}}]_{0,1}$ for air-filled Al and SiC shells with thickness $h/d = 1/40$, and $T_{0,1}$ of their equivalent effective fluids, shown as a function of $k_f d/2\pi$. Left panels show $[\mathcal{R}^{\mathcal{S}}]_{0,1}$ and $T_{0,1}$ on a linear scale, right panels on a log scale. Both the real (blue, orange) and imaginary (black, red) parts of the matrix elements are shown. Dashed lines plot the imaginary part of $T_{0,1}^{k\to 0}$. In effective-medium theory, (a)–(d) monopole elements with $q = 0$ derive B_{eff}, while (e)–(h) dipole elements with $q = 1$ derive ρ_{eff}. Panel (b) plots $|\,\text{Re}\,[\mathcal{R}^{\mathcal{S}}]_0|$ and $|\,\text{Re}\,T_0|$ due to a sign difference with respect to the imaginary parts.

where $\overline{B}_{\text{eff}}$ and $\overline{\rho}_{\text{eff}}$ are the bulk modulus and density of the effective fluid, and the over-line denotes normalization to water. Figure 1 shows the matrix elements $[\mathcal{R}^{\mathcal{S}}]_{0,1}$ for air-filled elastic shells and their effective fluid counterparts $T_{0,1}$ calculated over two decades in dimensionless wave number $k_f d/2\pi$. The calculations are carried out for two common elastic materials, aluminum and silicon carbide, and in both cases a thin shell thickness to outer diameter ratio $h/d = 1/40$ is used to explore the possibility of a high-B, low-ρ effective medium.

Figures 1(a)–1(d) and 1(e)–1(h) show, respectively, the MST elements $[\mathcal{R}^{\mathcal{S}}]_0$ and $[\mathcal{R}^{\mathcal{S}}]_1$. The shells' effective fluid properties derived from Eqs. (5) and (6) are used to calculate the exact T-matrix elements $T_{0,1}$ of the equivalent effective fluids; their lowest-order approximations $T_{0,1}^{k\to 0}$ are also shown as dashed lines. As $k_f d \to 0$, we observe the expected effective-medium behavior for the MST elements: $\text{Im}\,[\mathcal{R}^{\mathcal{S}}]_q \gg \text{Re}\,[\mathcal{R}^{\mathcal{S}}]_q$ and $[\mathcal{R}^{\mathcal{S}}]_q \to T_q^{k\to 0}$. However, as k_f increases above the long-wave limit, we observe that for both Al and SiC the real and imaginary parts of $[\mathcal{R}^{\mathcal{S}}]_q$ closely track those of the effective fluid elements T_q up to $k_f d \approx 2\pi$. Thus the effective fluid properties are a good approximation to the elastic shells even up to wavelengths on the order of the shell diameter. Most significantly, the effective

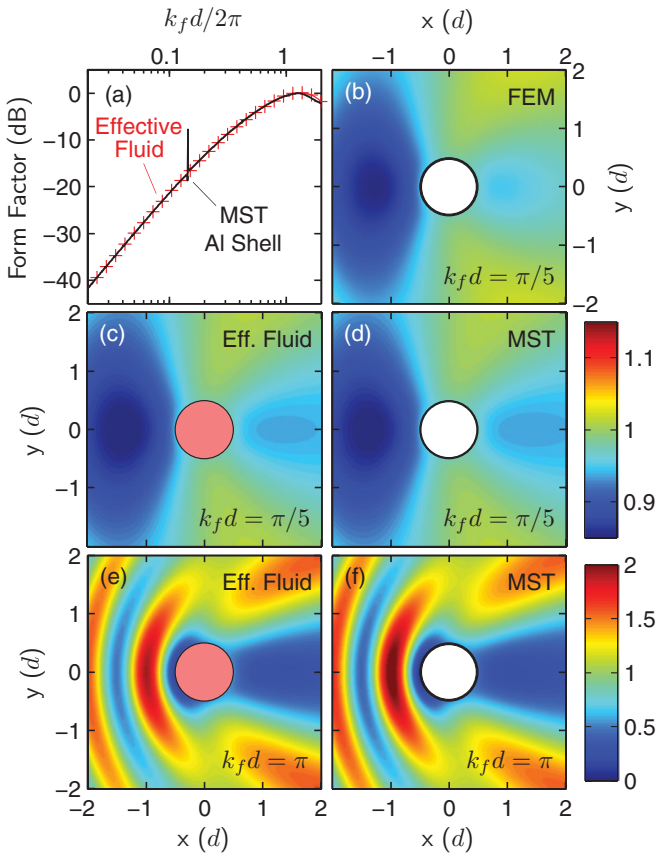

FIG. 2. (Color) (a) A comparison of the far-field form factors $F(k_f)$ for an air-filled Al shell with $h/d = 1/40$ and its equivalent effective fluid as a function of $k_f d/2\pi$. (b)–(f) Spatial maps of the near-field acoustic intensity demonstrate that the Al shell (b,d,f) is well approximated by its effective fluid (c,e) at two different wavelengths. Modes up to $|q| = 20$ are included.

properties obtained in Fig. 1 are high-B/low-ρ, resulting in $[\overline{B}_{\text{eff}},\overline{\rho}_{\text{eff}}] = [0.932,0.264]$ for Al and $[5.60,0.316]$ for SiC.

Figure 2 compares the near-field and far-field scattering of the Al shell from Fig. 1 to its equivalent effective fluid cylinder, calculated based on an incident plane wave in water. Figure 2(a) shows the far-field form factor,[15] $F(k_f) = (4/k_f)\sum_q |[\mathcal{R}^{\mathcal{S}}]_q|^2$, which quantifies the scattering in all directions. The $F(k_f)$ of the effective fluid (calculated using T_q) is indistinguishable from that of the Al shell for $k_f d \leqslant 2\pi$, with the exception of a few resonances at higher wave number. These shell resonances[30] are also observed at the same wave numbers in Fig. 1, but we emphasize that all are very narrow in bandwidth. Intensity maps in Figs. 2(c) and 2(d) show the near-field scattering at $k_f d = \pi/5$ and demonstrate almost identical behavior for the effective fluid and the Al shell. A finite element solution using COMSOL MULTIPHYSICS for the Al shell in Fig. 2(b) also conforms to the intensity map of the MST result. When scattering elements are brought together to form regular lattices, the homogenization condition is typically met for wavelengths $\lambda_f \gtrsim 4a$, where a is the lattice constant. In Figs. 2(e) and 2(f), there is little discernible difference between the near-field intensities of the Al shell and effective fluid at $\lambda_f = 2d$, indicating that elastic shells are viable candidates as components in homogenized metamaterials.

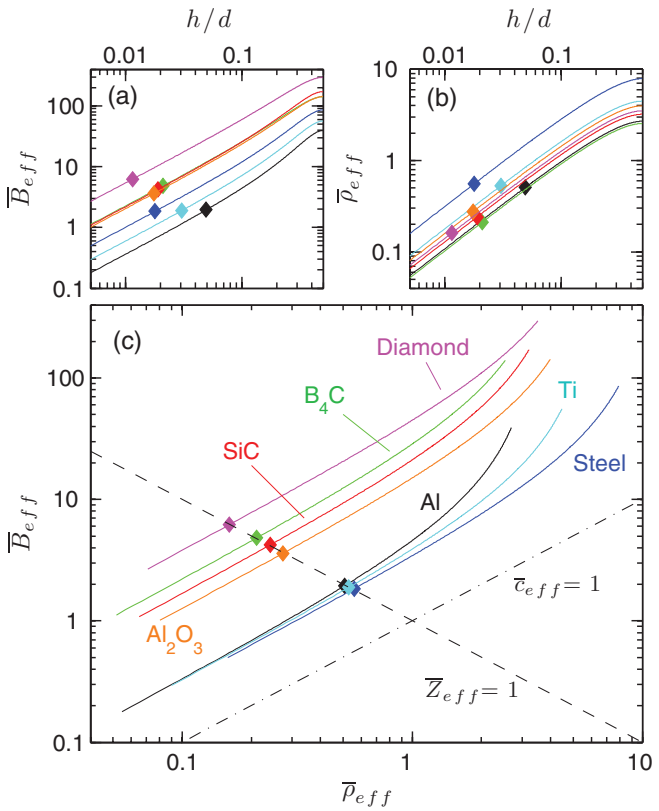

FIG. 3. (Color) (a) The effective bulk moduli $\overline{B}_{\text{eff}}$ and (b) densities $\overline{\rho}_{\text{eff}}$ of seven elastic shell materials (air cores) show a broad range of accessible properties as a function of shell thickness h/d. (c) The data from panels (a,b) are displayed in a $[\overline{B}_{\text{eff}},\overline{\rho}_{\text{eff}}]$ parameter space. Effective properties are normalized to water. Diamonds plot the $[\overline{B}_{\text{eff}},\overline{\rho}_{\text{eff}}]$ where each material is impedance-matched.

Figures 3(a) and 3(b) show $\overline{B}_{\text{eff}}$ and $\overline{\rho}_{\text{eff}}$ as a function of h/d for a number of common elastic materials with high sound speed relative to water; the core is filled with air in each case. For the shells we use material properties commonly found in the literature. Figure 3(c) shows the same data plotted in a $[\overline{B}_{\text{eff}},\overline{\rho}_{\text{eff}}]$ parameter space. The elastic shells' effective properties span a wide region of the parameter space where the sound speed is greater than water ($\overline{c}_{\text{eff}} > 1$), leading to extreme material properties not found in bulk materials. For a given $\overline{\rho}_{\text{eff}}$, ceramic shells offer a larger $\overline{B}_{\text{eff}}$ than metal shells. Once the shell material is chosen, however, the effective properties track lines roughly parallel with $\overline{c}_{\text{eff}} = 1$ as a function of h/d. As $h/d \to 1/2$, the trends for each material in Fig. 3 converge to a solid cylinder effective modulus, $B_s = (\lambda_s + \mu_s)$, in agreement with previous results for solid elastic cylinders;[31] λ_s and μ_s are the solid's Lamé constants.

Transparency is essential to many metamaterial applications,[7–10,12–15,17] and the incorporation of components that are themselves impedance-matched ($\overline{Z}_{\text{eff}} = 1$) should make transparency easier to achieve. Diamond symbols in Fig. 3 mark the h/d at which the effective properties become impedance-matched to water. All the solids explored in Fig. 3 attain $\overline{Z}_{\text{eff}} = 1$, and for solids with impedance larger than water a matched condition will be found for some h/d. As one might expect, the condition $\overline{Z}_{\text{eff}} = 1$ is obtained at lower $\overline{\rho}_{\text{eff}}$ as the elastic moduli of the shells increase. We emphasize that matched impedance is contingent only on the ratio h/d and is

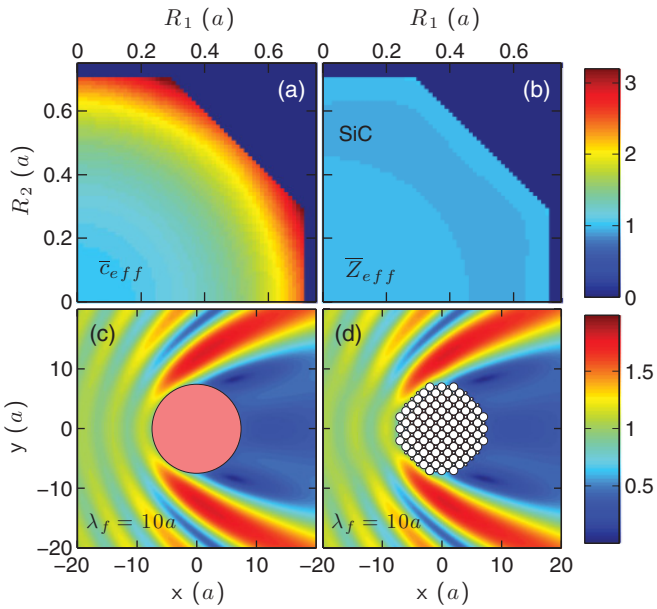

FIG. 4. (Color) (a) Effective sound speed $\overline{c}_{\text{eff}}$ and (b) impedance $\overline{Z}_{\text{eff}}$ for a square lattice of air-filled SiC shells with thickness $h/d = 1/50$, as a function of the outer radii R_1 and R_2 of its two-atom basis. h/d is kept constant in the two basis sites, but R_1 and R_2 vary independently thus changing the filling fraction. Near-field acoustic intensity maps demonstrate that (d) a circular-shaped lattice with $[R_1,R_2] = [0.25a,0.7a]$ (lattice constant a) is well approximated by (c) its equivalent effective fluid with properties $[\overline{c}_{\text{eff}},\overline{Z}_{\text{eff}}] = [3.10,0.998]$ derived from panels (a,b). Modes up to $|q| = 12$ are included.

independent of the outer diameter of the shell. Although the effective properties of the metal shells in Fig. 3(c) converge as $h/d \to 0$, leading to very similar effective properties at $\overline{Z}_{\text{eff}} = 1$, the impedance-matched ratio h/d is different for each metal. For example, $h/d \approx 1/20$ for Al as opposed to $1/56$ for stainless steel.

Figure 4 demonstrates that the elastic shells can be combined into a homogenized lattice[31,32] to create effective media with $\overline{Z}_{\text{eff}} = 1$. Figures 4(a) and 4(b) shows the achievable range of $\overline{c}_{\text{eff}}$ and $\overline{Z}_{\text{eff}}$ for a square lattice of air-filled SiC shells with impedance-matched ratio $h/d = 1/50$, calculated in the limit $k_f d \to 0$.[31] The axes are the outer radii R_1 and R_2 of shells in a mixed lattice with a "two-atom" basis.[31] The calculation is constrained by the fact that adjacent cylinders cannot overlap. $\overline{c}_{\text{eff}}$ increases with the cylinder filling fraction, reaching a maximum of $\overline{c}_{\text{eff}} \approx 3$. Crucially, because the constituent SiC shells are themselves impedance-matched, we obtain $\overline{Z}_{\text{eff}} \approx 1$ over the entire parameter space in Fig. 4(b).

Figures 4(c) and 4(d) compare the near-field acoustic intensity of a square lattice of SiC shells ($h/d = 1/50$) to the fluid cylinder that it approximates in the homogenization limit.[32] The square lattice has component radii $[R_1, R_2] = [0.25a, 0.7a]$ resulting in $[\overline{c}_{\text{eff}}, \overline{\rho}_{\text{eff}}] = [3.10, 0.322]$ and $\overline{Z}_{\text{eff}} = 0.998$. The acoustic intensity of the lattice is calculated using full MST,[31,32] and Eqs. (1)–(4) are used to calculate the stress within each SiC shell. The incident wavelength is $\lambda_f = 10a$, and the fluid cylinder is assigned the lattice's effective properties. The intensity map of the fluid cylinder is indistinguishable from that of the SiC shell lattice, demonstrating the equivalence of the effective media. The matched impedance results in a very low backscattered intensity. We emphasize that the acoustic properties of the SiC lattice are competitive with extraordinarily stiff composite materials reported in the literature.[16] For comparison with the metallic microlattices recently reported in Ref. 16, the SiC shell lattice has renormalized effective properties $[B_{\text{eff}}/B_s, \rho_{\text{eff}}/\rho_s] = [0.018, 0.10]$, where B_s and ρ_s are, respectively, the solid cylinder modulus and density of SiC. These properties would appear just above the trend for open-cell polymer foams on the far right side of Fig. 4 in Ref. 16.

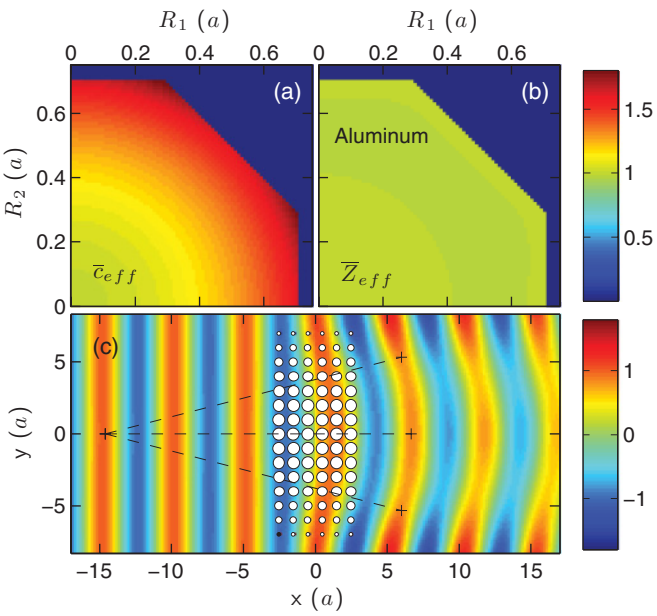

FIG. 5. (Color) (a) Effective sound speed $\overline{c}_{\text{eff}}$ and (b) impedance $\overline{Z}_{\text{eff}}$ for a square lattice of air-filled Al shells with thickness $h/d = 1/20$, as a function of the outer radii R_1 and R_2 of its two-atom basis. (c) The total pressure amplitude of a plane wave impinging on a concave graded index lens, composed of impedance-matched Al shells, shows a diverging wavefront leaving the lens. Dashed lines indicate the virtual focal length. Modes up to $|q| = 15$ are included.

Figures 5(a) and 5(b) show the achievable range of $\overline{c}_{\text{eff}}$ and $\overline{Z}_{\text{eff}}$ for a square lattice of impedance-matched, air-filled Al shells with $h/d = 1/20$. As was the case for SiC, the lattice is impedance-matched over the entire range of filling fractions. We utilize the parameter space in Figs. 5(a) and 5(b) to design a fully transparent gradient index lens in water.[17,31] For the case of Al shells, we are restricted to a concave lens because $\overline{c}_{\text{eff}} \geqslant 1$ at all filling fractions. The lens is designed using a concave graded index $\overline{n}_{\text{eff}}(y) = \overline{n}_0\sqrt{1+\alpha^2 y^2}$ by tuning the Al shell radii in stratified layers as a function of y.[17] We choose for our lens $\overline{n}_0 = 0.7$ and $\alpha = 0.133/a$, which results in a lens width $w_l = 15a$ and thickness $t_l = 6a$, where a is the lattice constant. Figure 5(c) shows the pressure amplitude of a plane wave impinging on the lens from the left with $\lambda_f \approx 5a$, calculated using MST both within and between the Al shells. It is evident that backscattering from the lens is almost zero, while the transmission becomes a diverging wavefront. The dashed lines map the expected positions of the wavefront based on a virtual focal length $f \approx 1/n_0\alpha \sin(\alpha t_l) \approx 15a$,[17] which clearly correlates well with the simulated wave.

To summarize, we have demonstrated that fluid-filled elastic shells can be utilized in aqueous environments as homogenized, low-dispersion scattering components for metamaterial applications, particularly those involving TA such as scattering reduction[7,8,14,15] and lensing[11,12] where tunable high-c, low-ρ material properties are sorely needed. Furthermore, it was shown that both isotropic and impedance-matching properties can be simultaneously obtained over a large bandwidth operating from a long-wavelength region down to the static limit. If required, changing the spatial distribution of different scatterers can attain a tunable material anisotropy. Lastly, a gradient index lens was conceptualized from the presented methods and was numerical shown to be highly transparent. Realization of such a lens will be greatly facilitated by the fact the shells are relatively simple to manufacture. While metamaterials are especially important to aqueous diagnostic applications because electromagnetic absorption is significant in fluids, we emphasize that our results extend to other acoustoelastic regimes. We believe the proposed method will provide a more straightforward approach to the design and realization of elastic wave metamaterials and TA devices in general, of which to date there are a only a few experimental cases. A similar procedure for three-dimensional structures can be similarly obtained, which will be explored elsewhere.

This work was supported by the US Office of Naval Research.

[1]J. Li, L. Fok, X. Yin, G. Bartal, and X. Zhang, Nat. Mater. **8**, 931 (2009).
[2]B.-I. Popa, L. Zigoneanu, and S. A. Cummer, Phys. Rev. Lett. **106**, 253901 (2011).
[3]V. M. García-Chocano, L. Sanchis, A. Díaz-Rubio, J. Martínez-Pastor, F. Cervera, R. Llopis-Pontiveros, and J. Sánchez-Dehesa, Appl. Phys. Lett. **99**, 074102 (2011).
[4]N. Stenger, M. Wilhelm, and M. Wegener, Phys. Rev. Lett. **108**, 014301 (2012).
[5]B. Liang, X. S. Guo, J. Tu, and J. C. Cheng, Nat. Mater. **9**, 989 (2010).
[6]X.-F. Li, X. Ni, L. Feng, M.-H. Lu, C. He, and Y.-F. Chen, Phys. Rev. Lett. **106**, 084301 (2011).
[7]H. Chen and C. T. Chan, Appl. Phys. Lett. **91**, 183518 (2007).
[8]S. A. Cummer, B.-I. Popa, D. Schurig, D. R. Smith, J. Pendry, M. Rahm, and A. Starr, Phys. Rev. Lett. **100**, 024301 (2008).
[9]A. N. Norris, Proc. R. Soc. London, Ser. A **464**, 2411 (2008).
[10]J. Hu, Z. Chang, and G. Hu, Phys. Rev. B **84**, 201101(R) (2011).
[11]C. Ren, Z. Xiang, and Z. Cen, Appl. Phys. Lett. **97**, 044101 (2010).
[12]C. N. Layman, T. P. Martin, K. M. Moore, D. C. Calvo, and G. J. Orris, Appl. Phys. Lett. **99**, 163503 (2011).
[13]R.-Q. Li, X.-F. Zhu, B. Liang, Y. Li, X.-Y. Zou, and J.-C. Cheng, Appl. Phys. Lett. **99**, 193507 (2011).
[14]H. Chen and C. T. Chan, J. Phys. D **43**, 113001 (2010).
[15]T. P. Martin and G. J. Orris, Appl. Phys. Lett. **100**, 033506 (2012).
[16]T. A. Schaedler, A. J. Jacobsen, A. Torrents, A. E. Sorensen, J. Lian, J. R. Greer, L. Valdevit, and W. B. Carter, Science **334**, 962 (2011).
[17]T. P. Martin, M. Nicholas, G. J. Orris, L.-W. Cai, D. Torrent, and J. Sánchez-Dehesa, Appl. Phys. Lett. **97**, 113503 (2010).
[18]A. E. H. Love, *A Treatise on the Mathematical Theory of Elasticity* (Cambridge University Press, Cambridge, 1906).
[19]A. Krynkin, O. Umnova, A. Y. B. Chong, S. Taherzadeh, and K. Attenborough, J. Acoust. Soc. Am. **128**, 3496 (2010).
[20]P. Lambin, A. Khelif, J. O. Vasseur, L. Dobrzynski, and B. Djafari-Rouhani, Phys. Rev. E **63**, 066605 (2001).
[21]M. Hirsekorn, Appl. Phys. Lett. **84**, 3364 (2004).
[22]X. Mei, G. Liu, Z. He, L. Yu, Z. Yu, and M. Ke, J. Appl. Phys. **107**, 064503 (2010).
[23]Y. A. Kosevich, C. Goffaux, and J. Sánchez-Dehesa, Phys. Rev. B **74**, 012301 (2006).
[24]Y. Ding, Z. Liu, C. Qiu, and J. Shi, Phys. Rev. Lett. **99**, 093904 (2007).
[25]X. Zhou and G. Hu, Phys. Rev. B **79**, 195109 (2009).
[26]Y. Wu, Y. Lai, and Z.-Q. Zhang, Phys. Rev. Lett. **107**, 105506 (2011).
[27]L.-W. Cai and J. Sánchez-Dehesa, J. Acoust. Soc. Am. **124**, 2715 (2008).
[28]L.-W. Cai, D. K. Dacol, G. J. Orris, D. C. Calvo, and M. Nicholas, J. Acoust. Soc. Am. **129**, 12 (2011).
[29]P. Sheng, *Introduction to Wave Scattering, Localization, and Mesoscopic Phenomena*, 2nd ed. (Springer-Verlag, Berlin, 2005).
[30]D. Torrent and J. Sánchez-Dehesa, New J. Phys. **13**, 093018 (2011).
[31]D. Torrent and J. Sánchez-Dehesa, New J. Phys. **9**, 323 (2007).
[32]D. Torrent, A. Hakansson, F. Cervera, and J. Sánchez-Dehesa, Phys. Rev. Lett. **96**, 204302 (2006).